New Journal of Physics
An Institute of Physics and Deutsche Physikalische Gesellschaft Journal

Dynamics of Bloch oscillations

T Hartmann, F Keck, H J Korsch and S Mossmann
FB Physik, University of Kaiserslautern, D-67653 Kaiserslautern, Germany
E-mail: korsch@physik.uni-kl.de

New Journal of Physics **6** (2004) 2
Received 4 October 2003
Published 14 January 2004
Online at http://www.njp.org/ (DOI: 10.1088/1367-2630/6/1/002)

Abstract. We study the dynamics of Bloch oscillations in a one-dimensional periodic potential plus a (relatively weak) static force. The tight-binding and single-band approximations are analysed in detail, and also in a classicalized version. A number of numerically exact results obtained from wavepacket propagation are analysed and interpreted in terms of the tight-binding and single-band model, both in co-ordinate and momentum space.

Contents

PII: S1367-2630(04)70006-3

1. Introduction

In this paper we will discuss in detail an elementary quantum system, namely the dynamics of a single particle in a one-dimensional periodic potential under the influence of a static force, i.e. the dynamics generated by the Hamiltonian

$$H = H_0 + Fx = \frac{p^2}{2M} + V(x) + Fx, \qquad V(x+d) = V(x). \tag{1}$$

The dynamics is non-intuitive: instead of the expected accelerated motion towards infinity, one observes a coherent oscillation with period

$$T_B = \frac{2\pi\hbar}{dF} \tag{2}$$

within a well-defined space interval of length L, which is inversely proportional to the force F. A simplistic explanation can be given by the invariance under a combined translation in space by one lattice period d and an energy shift $\delta E = Fd$, which leads to a phase shift $\delta E t/\hbar$, i.e. at a time T_B this phase equals 2π. Assuming in addition that the Bloch bands of the field-free system are simply tilted with a slope F, the available interval for a motion in the x-direction is reduced to

$$L = \Delta/F, \tag{3}$$

where Δ is the bandwidth. This simple tilted-band picture, which seems to go back to Zener's celebrated paper [1], provides an easy way to obtain a first information about dynamical features of the system. Essentially, the same ideas appear in the context of the 'acceleration theorem', where the starting point is again the field-free Bloch band picture. The quasi-momentum κ changes linearly with time, $\kappa(t) = \kappa(0) - Ft/\hbar$, until it reaches the boundary of the Bloch band, where it is Bragg-reflected. This picture dates back to the work of Bloch [2] and Zener [1]. For a recent discussion, see [3] and references therein; a recent rigorous derivation of the 'acceleration theorem' can be found in [4].

An alternative description is possible in terms of Wannier–Stark resonance states (see e.g. the review [5] and references therein). Let us just state here that the energy spectrum consists of ladders

$$\mathcal{E}_{\alpha,n} = \mathcal{E}_\alpha + ndF, \qquad \alpha \in \mathbb{N}_0, \quad n \in \mathbb{Z} \tag{4}$$

the Wannier–Stark ladders, where α denotes the different ladders and n the equidistant rungs. Moreover, the corresponding eigenstates, the Wannier–Stark states $\Psi_{\alpha,n}$, are resonance states and the energies (4) are complex-valued, where the imaginary part of $\mathcal{E}_\alpha$ gives the (reciprocal) lifetime. An efficient method for a numerical calculation of Wannier–Stark resonance energies can be found in [5, 6].

Figure 1 shows a schematic illustration of the potential $\cos x + Fx$ for a relatively strong field $F = 0.05$. The positions of the lowest three Wannier–Stark ladders are marked by lines whose thickness denotes the increasing width (the decreasing lifetime).

In view of the long history of the theoretical understanding of the dynamics of Wannier–Stark systems extending over many decades, an experimental investigation started only recently; however, it is quite intensive and in an increasing number of different

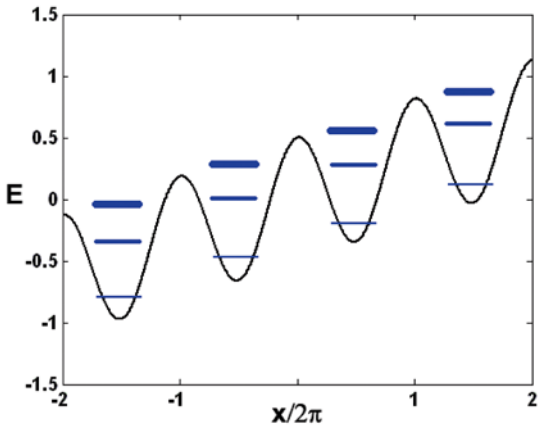

Figure 1. Schematic illustration of the Wannier–Stark ladders of resonances. The width of the lines indicate the width of the levels, i.e. their instability.

systems. Experimental evidence of Bloch oscillations can be found for electrons in solid state superlattices [7]–[11], for ultracold atoms in optical lattices, e.g. in the groups of Salomon [12]–[14] or Raizen [15]–[19] (see [20] for a review), for Bose–Einstein condensates [21]–[23], for photons in temperature-tuned waveguide arrays [24]–[28], and exponentially chirped Bragg gratings [29] and may also be observable for magnetic solitons [30]. In addition, the coupling of Bloch oscillations of electrons in superlattices to optical phonons has been studied [31].

Although various special aspects of Bloch oscillations have been investigated previously, the general features of the dynamics have not been treated before and the present paper therefore fills a gap in the literature.

2. Single-band tight-binding dynamics

Two related models allow an analytic treatment of the dynamics of Bloch oscillators and provide valuable insight, namely the tight-binding and single-band model. In their simplest form, these models entirely neglect the coupling between bands, i.e. Zener tunnelling, and therefore, of course, also the decay. In the following, we will briefly rederive the basic results, although in the not so well known momentum representation, which offers various advantages compared to the traditional approach. We restrict the discussion to the most simple case where only nearest-neighbour coupling is included. One should be aware of the fact, however, that a tight-binding model can include couplings of longer range as well as coupling between bands, e.g. in the analysis of Bloch oscillations in a two-band model [32].

2.1. Tight-binding model: basic features

Let us start with a brief discussion of the tight-binding model (for more details see [33, 34] and references therein) described by the Hamilton operator in terms of Wannier states $|n\rangle$ which are localized on the nth period of the potential, i.e. on 'site' n:

$$H = -\frac{\Delta}{4}\sum_{n=-\infty}^{+\infty}(|n\rangle\langle n+1| + |n+1\rangle\langle n|) + dF\sum_{n=-\infty}^{+\infty} n|n\rangle\langle n| \tag{5}$$

(to simplify the notation, throughout this subsection the band index α is suppressed). Note that in this model only neighbouring sites are directly coupled. Alternatively, one can use a representation in Bloch waves

$$|\kappa\rangle = \sum_{n=-\infty}^{+\infty} |n\rangle\langle n|\kappa\rangle = \sqrt{\frac{d}{2\pi}} \sum_{n=-\infty}^{+\infty} |n\rangle\, \mathrm{e}^{\mathrm{i}n\kappa d}, \tag{6}$$

which satisfy the Bloch condition $\langle n+1|\kappa\rangle = \mathrm{e}^{\mathrm{i}\kappa d}\langle n|\kappa\rangle$ with quasi-momentum κ confined to the Brillouin zone $-b/2 \leqslant \kappa \leqslant +b/2$ ($b = 2\pi/d$). By means of the identities

$$\begin{aligned}
\sum_{n=-\infty}^{+\infty} \langle\kappa'|n+1\rangle\langle n|\kappa\rangle &= \mathrm{e}^{-\mathrm{i}\kappa' d}\frac{d}{2\pi}\sum_{n=-\infty}^{+\infty}\mathrm{e}^{\mathrm{i}n(\kappa-\kappa')d} = \delta(\kappa'-\kappa)\mathrm{e}^{-\mathrm{i}\kappa d},\\
\sum_{n=-\infty}^{+\infty} n\langle\kappa'|n\rangle\langle n|\kappa\rangle &= \frac{d}{2\pi}\sum_{n=-\infty}^{+\infty} n\mathrm{e}^{\mathrm{i}n(\kappa-\kappa')d} = \delta(\kappa'-\kappa)\frac{\mathrm{i}}{d}\frac{\mathrm{d}}{\mathrm{d}\kappa},
\end{aligned} \tag{7}$$

we see that the tight-binding Hamiltonian (5) is diagonal, $\langle\kappa'|H|\kappa\rangle = d\delta(\kappa'-\kappa)H(\kappa)$, with

$$H(\kappa) = -\frac{\Delta}{2}\cos(\kappa d) + \mathrm{i}F\frac{\mathrm{d}}{\mathrm{d}\kappa}, \tag{8}$$

where the first term is the dispersion relation for the field-free case:

$$E(\kappa) = -\frac{\Delta}{2}\cos(\kappa d). \tag{9}$$

The eigenstates of the Hamiltonian (8), the Wannier–Stark states $|\Psi_m\rangle$, are immediately found by integrating the first-order differential equation

$$-\frac{\Delta}{2}\cos(\kappa d)\Psi(\kappa) + \mathrm{i}F\frac{\mathrm{d}\Psi(\kappa)}{\mathrm{d}\kappa} = E\Psi(\kappa) \tag{10}$$

with the periodic boundary condition $\Psi(\kappa+b) = \Psi(\kappa)$. This leads to the energies $E_m = mdF$, $m = 0, \pm1, \ldots$, the Wannier–Stark ladder and the corresponding eigenstates

$$\Psi_m(\kappa) = \langle\kappa|\Psi_m\rangle = \sqrt{\frac{d}{2\pi}}\mathrm{e}^{-\mathrm{i}[m\kappa d + \gamma\,\sin(\kappa d)]}, \qquad m = 0, \pm1, \ldots \tag{11}$$

with

$$\gamma = \Delta/2dF, \tag{12}$$

which are normalized with respect to the Brillouin zone $|\kappa| \leqslant b/2$. The time evolution operator $U(t)$ in the Bloch wave basis is simply

$$\begin{aligned}
U_{\kappa'\kappa}(t) = \langle\kappa'|U(t)|\kappa\rangle &= \sum_m \langle\kappa'|\Psi_m\rangle\, \mathrm{e}^{-\mathrm{i}E_m t/\hbar}\langle\Psi_m|\kappa\rangle\\
&= \frac{d}{2\pi}\mathrm{e}^{-\mathrm{i}\gamma[\sin\kappa' d - \sin\kappa d]}\sum_m \mathrm{e}^{-\mathrm{i}m(\kappa'-\kappa+Ft/\hbar)d}\\
&= \mathrm{e}^{-\mathrm{i}\gamma[\sin\kappa' d - \sin\kappa d]}\delta(\kappa'-\kappa+Ft/\hbar)
\end{aligned} \tag{13}$$

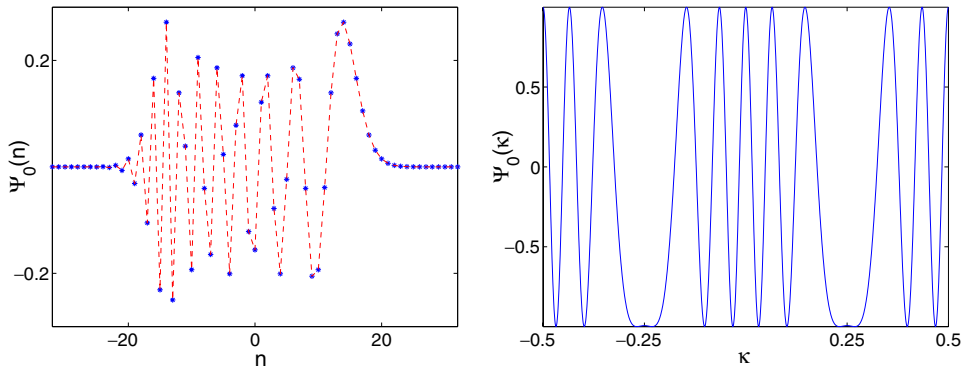

Figure 2. Wannier–Stark state Ψ_0 in the Wannier (left) and Bloch representation (right) for $\gamma = 15.8$.

where the reduction to the Brillouin zone $|\kappa| \leqslant b/2$ is understood. We see that the quasi-momentum κ' follows the classical acceleration

$$\kappa' = \kappa_t = \kappa - Ft/\hbar. \tag{14}$$

The description in terms of the Wannier states is a little bit more elaborate. Fourier transformation yields

$$\begin{aligned}\Psi_m(n) = \langle n|\Psi_m\rangle &= \int_{-b/2}^{+b/2} \mathrm{d}\kappa \langle n|\kappa\rangle\langle\kappa|\Psi_m\rangle = \frac{d}{2\pi}\int_{-b/2}^{+b/2} \mathrm{d}\kappa\, \mathrm{e}^{\mathrm{i}[(n-m)\kappa d - \gamma\sin(\kappa d)]} \\ &= \frac{1}{2\pi}\int_{-\pi}^{+\pi} \mathrm{d}u\, \mathrm{e}^{\mathrm{i}[(n-m)u - \gamma\sin u]} = J_{n-m}(\gamma)\end{aligned} \tag{15}$$

because of the integral representation of the Bessel function [35]. This provides the well-known Wannier–Stark states [33, 36] in the Wannier representation:

$$|\Psi_m\rangle = \sum_n J_{n-m}(\gamma)|n\rangle. \tag{16}$$

Figure 2 shows, as an illustrative example, the Wannier–Stark states in the Wannier and Bloch representation for parameters $\Delta = 0.994$, $d = 2\pi$ and $F = 0.005$, i.e. $\gamma = 15.8$, which is related to the experimental results in [21] and is also used in the exact numerical computations discussed in section 3. From the properties of the Bessel functions [35], we know that $J_{n-m}(\gamma)$ is mainly localized in the interval $|m - n| < \gamma$, i.e. the Wannier–Stark states extend over an interval

$$L = 2\gamma d = \Delta/F \tag{17}$$

as already stated in (3). Outside this interval, the Bessel functions decay as $J_n(\gamma) \sim \gamma^n$. Furthermore, the Bessel functions strongly oscillate for negative values of the index because of the property $J_{-n}(z) = (-1)^n J_n(z)$. We will see that the spatial extension of the Wannier–Stark state determines the boundaries of the Bloch oscillations.

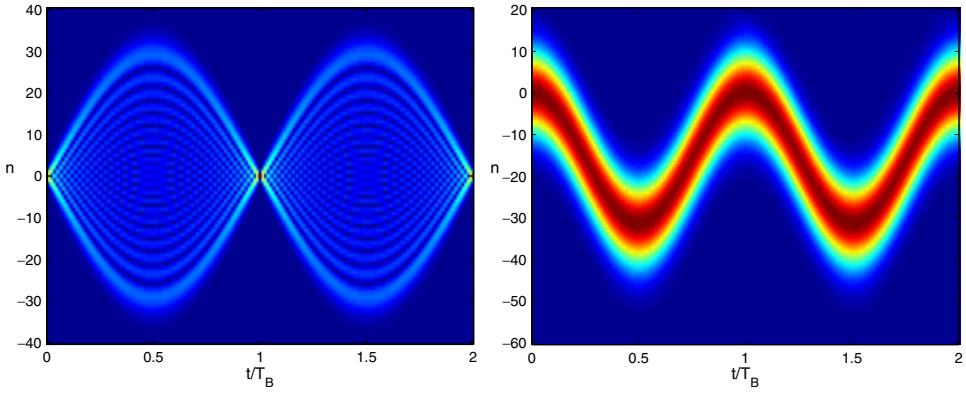

Figure 3. Breathing mode for a state initially localized at $n = 0$ (left) and oscillatory mode for an extended Gaussian distribution (22) with $\beta = 0.01$ (right) in the tight-binding model with $\gamma = 15.8$. Shown is a colour map of $|\langle n|\psi(t)\rangle|$ as a function of t/T_B and n.

In the basis of Wannier states one obtains the propagator as [33, 36]

$$U_{nn'}(t) = \langle n|U(t)|n'\rangle = \sum_l \langle n|\Psi_l\rangle e^{-iE_l t/\hbar}\langle \Psi_l|n'\rangle$$
$$= J_{n-n'}\left(2\gamma \sin\frac{\omega_B t}{2}\right) e^{i(n-n')(\pi-\omega_B t)/2 - in'\omega_B t}, \tag{18}$$

the Fourier image of (13). Here $\omega_B = 2\pi/T_B = dF/\hbar$ is the Bloch frequency. The time evolution operator is periodic with the Bloch period $T_B = 2\pi\hbar/(dF)$. It should be noted that this analysis can also be extended to the case of a time-dependent force $F(t)$ [33, 37, 38].

Let us consider two illustrating limits of the dynamics generated by (18). For an initial state

$$|\psi(t)\rangle = \sum_n c_n(t)|n\rangle, \qquad \sum_n |c_n|^2 = 1, \tag{19}$$

which is strongly localized in co-ordinate space, e.g. in the extreme case $c_n(0) = \delta_{n0}$ where a single Wannier state $n = 0$ is populated at time $t = 0$, the time dependence is

$$c_n(t) = U_{n0}(t) = J_n\left(2\gamma \sin\frac{\omega_B t}{2}\right) e^{in(\pi-\omega_B t)/2}. \tag{20}$$

In such a breathing mode, the wavepackets widen and shrink periodically populating an interval

$$|n| < 2\gamma\left|\sin\frac{\omega_B t}{2}\right| \tag{21}$$

(index of the Bessel function smaller than its argument). Figure 3 shows such a breathing oscillation, again for parameter $\gamma = 15.8$ used already in figure 2.

In the other extreme of a broad Gaussian wavepacket,

$$c_n(0) = g\ \exp(-\beta n^2 + in\kappa_0 d) \tag{22}$$

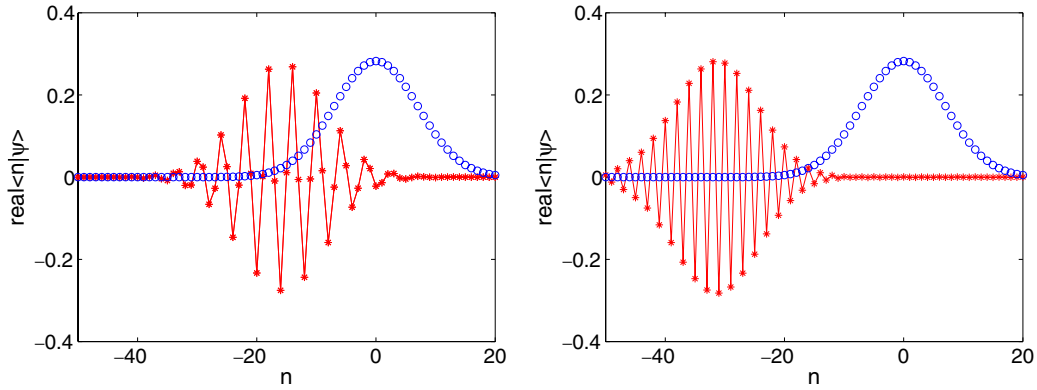

Figure 4. Real part of the wavefunction $\langle n|\psi(t)\rangle$ (red $*$) for a broad initial Gaussian with distribution (22) with $\beta = 0.01$ in the tight-binding model with $\gamma = 15.8$ for times $t = T/4$ (left) and $T/2$ (right). Also shown is the initial distribution (blue o).

(g is a normalization factor) with small β, the time evolution of the coefficients is approximately given by

$$c_n(t) \approx g\ \exp(-\mathrm{i}\Phi(t) + \mathrm{i}n(\kappa_0 d - \omega_B t) - \beta(n - n(t))^2) \tag{23}$$

(see [33] for details), i.e. a Gaussian with wavenumber $\kappa_t = \kappa - Ft/\hbar$, as already found in (14), whose centre performs a Bloch oscillation:

$$n(t) = \gamma[\cos(\kappa_0 d - \omega_B t) - \cos(\kappa_0 d)] = -2\gamma \sin\frac{\omega_B t}{2}\sin\left(\frac{\omega_B t}{2} - \kappa_0 d\right). \tag{24}$$

$\Phi(t)$ is the dynamical phase well known from the discussion of an adiabatic evolution of eigenstates in systems with parameter-dependent Hamiltonians:

$$\begin{aligned}\Phi(t) &= \frac{1}{\hbar}\int_0^t E(\kappa_{t'})\,\mathrm{d}t' = -\frac{1}{F}\int_{\kappa_0}^{\kappa_0 - Ft/\hbar} E(\kappa)\,\mathrm{d}\kappa \\ &= -2\gamma \sin\frac{\omega_B t}{2}\cos\left(\frac{\omega_B t}{2} - \kappa_0 d\right)\end{aligned} \tag{25}$$

for the dispersion relation $E(\kappa)$ given in (9). An example is shown in figure 3. The amplitude of this oscillation, γ, is half of the amplitude of the breathing mode and the width of the wavepacket is almost constant, as will be discussed in more detail in section 2.2. Note that, in this case, the momentum distribution is sharply localized at $\kappa_0 = 0$, whereas it is extended in the case of a breathing mode.

The absolute value of the wavefunction shown in figure 3 does not resolve an important difference between the left and the right turning points of the Bloch oscillation, which is due to the variation of the phase. Figure 4 shows the real part of the wavefunction for a broad initial Gaussian distribution (22) with $\beta = 0.01$ after a quarter and half of a Bloch period. In particular, at $t = T_B/2$, the wavefunction is real and changes sign from one site to the next because of the phase term $\mathrm{e}^{\mathrm{i}n\omega_B t} = (-1)^n$. Note also a similar behaviour of the Wannier–Stark state shown in figure 2.

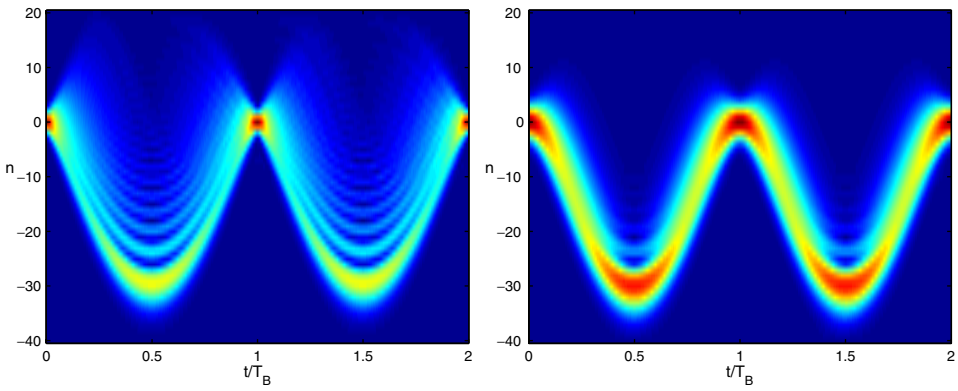

Figure 5. Bloch oscillation for Gaussian distributions (22) with $\beta = 0.3$ (left) and 0.1 (right) in the tight-binding model with $\gamma = 15.8$. Shown is a colour map of $|\langle n|\psi(t)\rangle|$ as a function of t/T_B and n.

For distributions which are not sharply localized in momentum or position, an intermediate behaviour is found, as illustrated in figure 5. In closing this subsection it should be noted that the analytical treatment of the tight-binding model can also be extended to the case where the force is explicitly time-dependent, $F = F(t)$, for example $F(t) = F_0 + F_1 \sin(\omega t)$ (a combined dc–ac Stark system), where the case ω/ω_B rational is of particular interest (see e.g. [33]).

2.2. Tight-binding model: expectation values

Important features of the dynamics of Bloch oscillations can be understood in terms of the time dependence of the mean position and momentum as well as their variances. In particular, for the tight-binding model, some analytical expressions have been derived both for time-dependent and -independent forces [33, 34, 37, 39, 40] using different techniques. Here, we will follow an algebraic derivation suggested recently [38] which allows a straightforward calculation of the quantities of interest.

The tight-binding Hamiltonian (8) may also be written as

$$\hat{H} = -\frac{\Delta}{2}\cos(\hat{\kappa}d) + F\hat{x}, \tag{26}$$

where $\hat{\kappa}$ and $\hat{x} = \mathrm{i}\mathrm{d}/\mathrm{d}\kappa$ are operators satisfying the commutation rule $[\hat{x}, \hat{\kappa}] = \mathrm{i}$. Inevitably, however, one encounters the well-known difficulties related to inconsistencies in the definition of angle operators (see e.g. [41, 42] and references therein). We therefore prefer to use the unitary operators [42]

$$\hat{K} = \exp(-\mathrm{i}\hat{\kappa}d) = \sum_{n=-\infty}^{+\infty} |n\rangle\langle n+1|, \qquad \hat{K}|n\rangle = |n-1\rangle \tag{27}$$

and $\hat{K}^\dagger$. With

$$\hat{x} = d\hat{N} = d\sum_{n=-\infty}^{+\infty} n|n\rangle\langle n|, \tag{28}$$

the tight-binding Hamiltonian is

$$\hat{H} = -\frac{\Delta}{4}(\hat{K} + \hat{K}^\dagger) + dF\hat{N}. \tag{29}$$

Using the commutators

$$[\hat{K}, \hat{N}] = \hat{K}, \qquad [\hat{K}^\dagger, \hat{N}] = -\hat{K}^\dagger, \qquad [\hat{K}, \hat{K}^\dagger] = 0, \tag{30}$$

one can easily solve the Heisenberg equations of motion for a general time-dependent force $F = F(t)$. Here we are aiming at a calculation of the time dependence of the expectation values.

For a normalized initial state which can be written as a linear combination of Wannier or Bloch states,

$$|\psi\rangle = \sum_n c_n |n\rangle = \int_{-b/2}^{+b/2} \mathrm{d}\kappa\, c(\kappa)|\kappa\rangle \tag{31}$$

the expectation value of $\hat{K}$ is the coherence parameter

$$K = |K|\,\mathrm{e}^{\mathrm{i}\kappa_0 d} = \langle\psi|\hat{K}|\psi\rangle = \sum_n c^*_{n-1}c_n = \int_{-b/2}^{+b/2} \mathrm{d}\kappa\, |c(\kappa)|^2\,\mathrm{e}^{\mathrm{i}\kappa d} \tag{32}$$

(the phase of the expectation value is used to *define* κ_0).

The time evolution

$$\dot{\hat{K}}_t = \frac{\mathrm{i}}{\hbar}[\hat{H}, \hat{K}_t] = \frac{\mathrm{i}dF}{\hbar}[\hat{N}_t, \hat{K}_t] = -\frac{\mathrm{i}dF}{\hbar}\hat{K}_t \tag{33}$$

can be solved immediately:

$$\hat{K}_t = \mathrm{e}^{-\mathrm{i}\eta_t}\hat{K} \quad \text{with} \quad \eta_t = \frac{d}{\hbar}\int_0^t \mathrm{d}t' F(t'). \tag{34}$$

Using $\hat{K}^\dagger_t = \mathrm{e}^{+\mathrm{i}\eta_t}\hat{K}^\dagger$ we obtain

$$\dot{\hat{N}}_t = \frac{\mathrm{i}}{\hbar}[\hat{H}_t, \hat{N}_t] = -\frac{\mathrm{i}\Delta}{4\hbar}[\hat{K}_t + \hat{K}^\dagger_t, \hat{N}_t] = -\frac{\mathrm{i}\Delta}{4\hbar}(\hat{K}_t - \hat{K}^\dagger_t) \tag{35}$$

and finally

$$\hat{N}_t = \hat{N} - \frac{\mathrm{i}\Delta}{4\hbar}(E_t\hat{K} - E^*_t\hat{K}^\dagger) \quad \text{with} \quad E_t = \int_0^t \mathrm{d}t'\,\mathrm{e}^{-\mathrm{i}\eta_{t'}}. \tag{36}$$

The expectation values are therefore

$$\langle\hat{K}\rangle_t = \mathrm{e}^{-\mathrm{i}\eta_t}\langle\hat{K}\rangle_0 = \mathrm{e}^{-\mathrm{i}(\eta_t - \kappa_0 d)}\,|K|, \tag{37}$$

$$\begin{aligned}\langle\hat{N}\rangle_t &= \langle\hat{N}\rangle_0 - \frac{\mathrm{i}\Delta}{4\hbar}|K|(E_t\,\mathrm{e}^{\mathrm{i}\kappa_0 d} - E_t^*\,\mathrm{e}^{-\mathrm{i}\kappa_0 d}) \\ &= \langle\hat{N}\rangle_0 - \frac{\mathrm{i}\Delta}{4\hbar}|K|\left(\int_0^t \mathrm{d}t'\,\mathrm{e}^{\mathrm{i}(\kappa_0 d-\eta_{t'})} - \int_0^t \mathrm{d}t'\,\mathrm{e}^{-\mathrm{i}(\kappa_0 d-\eta_{t'})}\right) \\ &= \langle\hat{N}\rangle_0 + \frac{\Delta}{2\hbar}|K|\int_0^t \mathrm{d}t'\sin(\kappa_0 d-\eta_{t'}) \\ &= \langle\hat{N}\rangle_0 - \frac{\Delta}{2\hbar}|K|(v_t\cos\kappa_0 d - u_t\sin\kappa_0 d) \end{aligned} \tag{38}$$

with

$$u_t = \int_0^t \mathrm{d}t'\cos\eta_{t'}, \qquad v_t = \int_0^t \mathrm{d}t'\sin\eta_{t'}. \tag{39}$$

For the case of constant F we have $\eta_t = \omega_B t$ and these expressions reduce to

$$u_t = \frac{1}{\omega_B}\sin\omega_B t, \qquad v_t = \frac{1}{\omega_B}(1-\cos\omega_B t) \tag{40}$$

and (38) can be rewritten as

$$\langle\hat{N}\rangle_t = \langle\hat{N}\rangle_0 - 2\gamma|K|\sin\frac{\omega_B t}{2}\sin\left(\frac{\omega_B t}{2} - \kappa_0 d\right). \tag{41}$$

For the example of a Gaussian distribution (22) this is simply the dynamics of its centre $n(t)$ given in (24) multiplied by $|K|$.

In the same way, one can derive analytic expressions for K_t^2, N_t^2 and for their expectation values. Introducing the abbreviations

$$L = |L|\,\mathrm{e}^{\mathrm{i}\nu} = \sum_n c_{n-2}^* c_n = \int_{-b/2}^{+b/2}\mathrm{d}\kappa\,|c(\kappa)|^2\,\mathrm{e}^{2\mathrm{i}\kappa d}, \tag{42}$$

$$J = \sum_n (2n-1)c_{n-1}^* c_n = |J|\,\mathrm{e}^{\mathrm{i}\mu} \tag{43}$$

we find

$$\langle\hat{K}^2\rangle_t = \mathrm{e}^{-2\mathrm{i}\eta_t}\langle\hat{K}^2\rangle_0 = \mathrm{e}^{-2\mathrm{i}\eta_t}\,L \tag{44}$$

and after some algebra

$$\begin{aligned}\langle\hat{N}^2\rangle_t = \langle\hat{N}^2\rangle_0 &+ \frac{\Delta^2}{8\hbar^2}[u_t^2 + v_t^2 - |L|\{(u_t^2 - v_t^2)\cos\nu + 2u_t v_t\sin\nu\}] \\ &+ \frac{\Delta}{2\hbar}|J|\,[u_t\sin\mu - v_t\cos\mu]. \end{aligned} \tag{45}$$

The equations for the expectation values simplify for a time-independent force F:

$$\langle N^2\rangle_t = \langle N^2\rangle_0 + 2\gamma^2\sin^2\frac{\omega_B t}{2}(1 - |L|\cos(\omega_B t - \nu)) + 2\gamma|J|\sin\frac{\omega_B t}{2}\sin\left(\mu - \frac{\omega_B t}{2}\right), \tag{46}$$

where γ is as defined in (12).

It is illuminating to look at two limiting cases. If, initially, only a single site $n = 0$ is populated, we have $\langle N\rangle_0 = \langle N^2\rangle_0 = 0$ and therefore with $K = L = J = 0$

$$\langle N\rangle_t = 0, \tag{47}$$

$$\Delta N_t = \frac{\Delta}{2\sqrt{2}\hbar}\sqrt{u_t^2 + v_t^2} \tag{48}$$

and for time-independent F

$$\Delta N_t = \sqrt{2}\gamma\left|\sin\frac{\omega_B t}{2}\right|, \tag{49}$$

i.e. the mean position is constant in time and the width oscillates with an amplitude in agreement with the estimate (21) for the breathing mode.

The other limiting case is a broad Gaussian distribution (22). In this case, the sums in (32), (42) and (43) can be replaced by integrals and we have

$$K \approx \mathrm{e}^{-\beta/2+\mathrm{i}\kappa_0 d}, \qquad L \approx \mathrm{e}^{-2\beta+\mathrm{i}2\kappa_0 d}, \qquad |J| \approx 0, \tag{50}$$

i.e. $|K| \approx |L| \approx 1$ and $\nu \approx 2\kappa_0 d$. Therefore, the expectation value (38) is

$$\langle\hat{N}\rangle_t = -\frac{\Delta}{2\hbar}(v_t\cos\kappa_0 d - u_t\sin\kappa_0 d) \tag{51}$$

and from (45) we get

$$\begin{aligned}\langle\hat{N}^2\rangle_t &= \langle\hat{N}^2\rangle_0 + \frac{\Delta^2}{8\hbar^2}[u_t^2 + v_t^2 - (u_t^2 - v_t^2)\cos(2\kappa_0 d) - 2u_t v_t\sin(2\kappa_0 d)]\\ &= \langle\hat{N}^2\rangle_0 + \frac{\Delta^2}{4\hbar^2}[v_t\cos(\kappa_0 d) - u_t\sin(\kappa_0 d)]^2\\ &= \langle\hat{N}^2\rangle_0 + [\langle\hat{N}\rangle_t]^2\end{aligned} \tag{52}$$

so that the width is constant in time:

$$(\Delta N_t)^2 = \langle\hat{N}^2\rangle_t - [\langle\hat{N}\rangle_t]^2 = \langle\hat{N}^2\rangle_0. \tag{53}$$

2.3. Single-band approximation

The single-band approximation is most conveniently formulated in the Bloch wave representation. Basically, the Hamiltonian (1) and the wavefunctions are expanded in terms of the Bloch states $|\varphi_{\alpha,\kappa}\rangle$ of the field-free Hamiltonian H_0 and the interband coupling and some part of the intraband coupling are neglected (see e.g. [4, 43] for more details). In the following we will skip the band index α. The resulting Hamiltonian

$$H(\kappa) = E(\kappa) + \mathrm{i}F\frac{\mathrm{d}}{\mathrm{d}\kappa} \tag{54}$$

closely resembles the tight-binding one (8), where the cosine-dispersion relation (9) is replaced by the dispersion relation $E(\kappa)$ of H_0. Here we confine ourselves again to the case of constant F.

Solving (54) for the eigenstates periodic in κ with period $b = 2\pi/d$ directly leads to the quantized Wannier–Stark eigenvalues

$$E_n = \int_{-b/2}^{b/2} E(\kappa)\,\mathrm{d}\kappa + ndF, \qquad n = 0, \pm 1, \pm 2, \ldots, \tag{55}$$

the Wannier–Stark ladder in the single-band approximation.

If we represent an arbitrary state in the basis of Bloch states with time-dependent expansion coefficients $c_\alpha(\kappa, t)$, the time-dependent single-band Schrödinger equation reads

$$\mathrm{i}\hbar\frac{\partial c(\kappa,t)}{\partial t} = E(\kappa)c(\kappa,t) + \mathrm{i}F\frac{\partial c(\kappa,t)}{\partial \kappa} \tag{56}$$

with solution

$$c(\kappa,t) = c(\kappa + Ft/\hbar, 0)\,\exp\left(-\frac{\mathrm{i}}{\hbar}\int_0^t E(\kappa(t'))\,\mathrm{d}t'\right) \tag{57}$$

as already postulated by Houston in 1940 [44] in the form

$$\varphi_\kappa(k,t) = \varphi_{\kappa - Ft/\hbar}(k)\,\exp\left(-\frac{\mathrm{i}}{F}\int_{\kappa - Ft/\hbar}^{\kappa} E(\kappa')\,\mathrm{d}\kappa'\right). \tag{58}$$

The expectation values for $\langle N\rangle_t$ and $\langle N^2\rangle_t$ have been derived by Grecchi and Sacchetti [4] in the limit of small F:

$$\langle N\rangle_t = \langle N\rangle_0 + \int_{-b/2}^{+b/2} \mathrm{d}\kappa\,|c(\kappa)|^2\,\Xi_t(\kappa) \tag{59}$$

with

$$\Xi_t(\kappa) = \frac{1}{dF}[E(\kappa) - E(\kappa - Ft/\hbar)] \tag{60}$$

and

$$\langle N^2\rangle_t = \langle N^2\rangle_0 + \int_{-b/2}^{+b/2} \mathrm{d}\kappa\,|c(\kappa)|^2[\Xi_t(\kappa)]^2. \tag{61}$$

These formulae agree with (41) and (46) for the tight-binding dispersion relation (9) in the limit of small F.

2.4. Classicalization

In this section, we will discuss the *classical* dynamics generated by the tight-binding Hamiltonian (26) by replacing the operators $\hat{x}$ and $\hat{\kappa}$ by real numbers x and $\kappa = p/\hbar$, where p has

the dimension of a momentum. Here

$$H = -\frac{\Delta}{2}\cos(p\delta) + Fx \tag{62}$$

with $\delta = d/\hbar$ appears as a Hamiltonian function in such a 'classicalization'. One should be aware of the fact that this classical dynamics explicitly depends on $\hbar$. Clearly, a classical version of the single-band model can be generated by replacing the tight-binding dispersion relation $-(\Delta/2)\cos(\kappa d)$ by the dispersion function $E(\kappa)$. In addition, one can extend the classical dynamics to time-dependent forces. Here we will, however, confine ourselves to the simplest case of constant F.

The solution of Hamilton's equations of motion

$$\dot{x}(t) = \frac{\partial H}{\partial p} = \frac{\Delta\delta}{2}\sin(p\delta), \qquad \dot{p}(t) = -\frac{\partial H}{\partial x} = -F \tag{63}$$

with initial conditions (p_0, x_0) at $t = 0$ are

$$x(t) = x_0 - \frac{\Delta}{F}\sin\frac{\omega_B t}{2}\sin\left(\frac{\omega_B t}{2} - p_0\delta\right), \qquad p(t) = p_0 - Ft, \tag{64}$$

where $\omega_B = F\delta$ is the Bloch frequency. Let us discuss the dynamics of an initial Gaussian distribution centred at (p_0, x_0) in phase space,

$$W(p, x, t = 0) = (2\pi\Delta x_0 \Delta p_0)^{-1} \exp\left[-\frac{(x - x_0)^2}{2\Delta x_0^2} - \frac{(p - p_0)^2}{2\Delta p_0^2}\right]. \tag{65}$$

The time dependence of the mean momentum and the momentum width is trivial:

$$\langle p\rangle_t = p_0 - Ft, \qquad \Delta p_t^2 = \Delta p_0^2, \tag{66}$$

the time evolution of the mean position is given by

$$\langle x\rangle_t = x_0 - \frac{\Delta}{F}\,\mathrm{e}^{-\Delta p_0^2\delta^2/2}\sin\frac{\omega_B t}{2}\sin\left(\frac{\omega_B t}{2} - p_0\delta\right) \tag{67}$$

and the time-dependent mean width reads

$$(\Delta x_t)^2 = (\Delta x_0)^2 + \frac{\Delta^2}{2F^2}(1 - \mathrm{e}^{-\Delta p_0^2\delta^2})\sin^2\frac{\omega_B t}{2}. \tag{68}$$

From these two equations we can see the following: both $\langle x\rangle_t$ and Δx_t are periodic functions of time with the Bloch period. The amplitude of the oscillation around the mean values is—as anticipated from quantum dynamics—determined by the momentum width. If this width is small, i.e. if we have a strongly localized initial momentum distribution, then $\exp(-\Delta p_0^2\delta^2) \approx 1$ and we observe a constant width and an oscillating mean value which can be interpreted as a 'classical' Bloch oscillation. In the opposite case, i.e. if the momentum

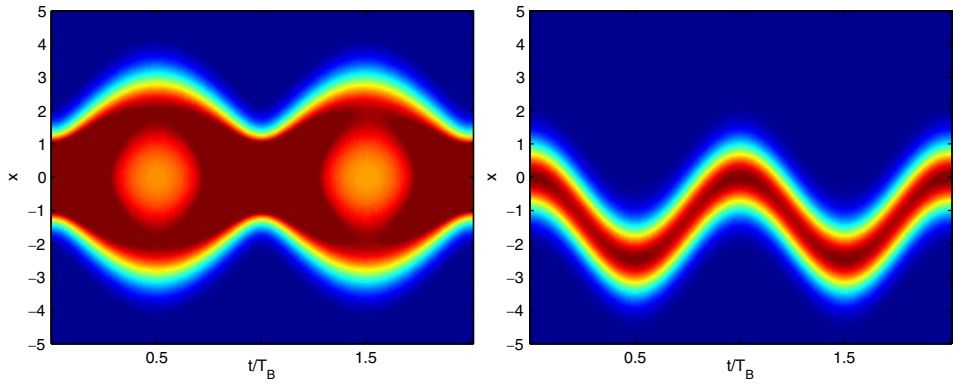

Figure 6. Classical Bloch oscillations. Shown is a breathing mode for $\Delta p_0 = 5$ (left) and an oscillatory mode for $\Delta p_0 = 0.2$ (right).

distribution is broad, we get $\exp(-\Delta p_0^2 \delta^2) \approx 0$ which leads to a nearly constant mean value $\langle x \rangle_t$ and an oscillating width Δx_t, a classical breathing mode.

This classical behaviour closely parallels the quantum case. The interference oscillations are, of course, absent here, but the classical mean value agrees with the quantum case (41). In the Gaussian approximation (50), we find with $\beta \approx 1/4\Delta n_0^2 = d^2/4\Delta x_0^2$ and $\Delta x_0 \Delta p_0 = \hbar/2$

$$|K| \approx \mathrm{e}^{-\beta/2} \approx \mathrm{e}^{-\Delta p_0^2 \delta^2/2} \tag{69}$$

in full agreement with (67).

Figure 6 shows a numerical example of classical Bloch oscillations both for a breathing and an oscillatory mode.

2.5. *Momentum distributions*

In the tight-binding and single-band model, one typically uses the Wannier states $|n\rangle$ or the Bloch states $|\kappa\rangle$. In many discussions, one can simply treat n as a substitute of the position co-ordinate x and κ for the wavenumber k. The first substitution is not critical because of the localization properties of the Wannier states in position space ($\psi_n(x) = \langle x|n\rangle$ is exponentially localized on site n [45]). Therefore the wavefunction in position space

$$\psi(x) = \sum_n c_n \psi_n(x) \tag{70}$$

appears as a locally smoothed version of the discrete distribution $\sum_n c_n \delta(x - nd)$ and a continuous Wannier–Stark wave function $\Psi_m(x)$ will be quite similar to the discrete version $\Psi_m(n)$ shown in figure 2.

For the momentum, however, the situation is different and it is important to distinguish between the quasi-momentum κ and the 'true' momentum k. It is elementary to prove the relations

$$\psi_n(k) = \langle k|n\rangle = \mathrm{e}^{-\mathrm{i}mkd} \psi_0(k), \tag{71}$$

$$\varphi_\kappa(k) = \langle k|\kappa\rangle = \sqrt{\frac{2\pi}{d}} \psi_0(k) \sum_n \delta(k - \kappa - nb) \tag{72}$$

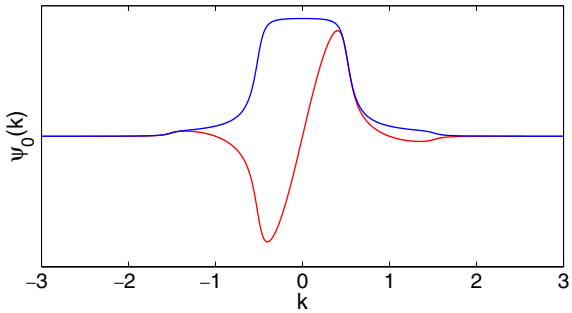

Figure 7. Wannier state $\psi_0(k)$ in the momentum representation for the potential $V(x) = \cos x$. Shown are the absolute value and the real part.

for the momentum representation of the Wannier or Bloch states. An example of the momentum representation of a Wannier state is shown in figure 7. The momentum distribution of an arbitrary state with Bloch representation

$$|\psi\rangle = \int_{-b/2}^{+b/2} \mathrm{d}\kappa c(\kappa)|\kappa\rangle \tag{73}$$

is therefore

$$\psi(k) = \langle k|\psi\rangle = \sqrt{\frac{2\pi}{d}}\psi_0(k)\sum_n c(k - nb). \tag{74}$$

Hence these distributions are determined by the envelope function $|\psi_0(k)|$, which is mainly localized in the interval $|k| < b/2$, the Brillouin zone, and decays rapidly outside this region. This envelope function is multiplied by periodically repeated copies of the quasi-momentum distribution $c(\kappa)$.

Within the tight-binding model, one can furthermore write down the following simple relation for the momentum representation of the Wannier–Stark states:

$$\Psi_m(k) = \mathrm{e}^{-\mathrm{i}mkd}\Psi_0(k) = \mathrm{e}^{-\mathrm{i}[mkd+\gamma\sin(kd)]}\psi_0(k), \tag{75}$$

where the phase factor is periodic in k with period b and the envelope function is again given by the Wannier distribution $|\psi_0(k)|$.

3. Wavepacket propagation

In this section, we discuss the dynamics of wavepackets in the limit of a weak field where the decay can be neglected, but beyond the tight-binding or single-band approximation. Similar studies have been carried out by Bouchard and Luban [46] with a view towards electrons in superlattices.

As an example, we assume a cosine potential, which quite naturally appears for atom dynamics in optical lattices. The time-dependent Schrödinger equation

$$\mathrm{i}\hbar\frac{\partial\psi}{\partial t} = -\frac{\hbar^2}{2M}\frac{\partial^2\psi}{\partial x^2} + (V_0\cos(2\pi x/d) + Fx)\psi, \tag{76}$$

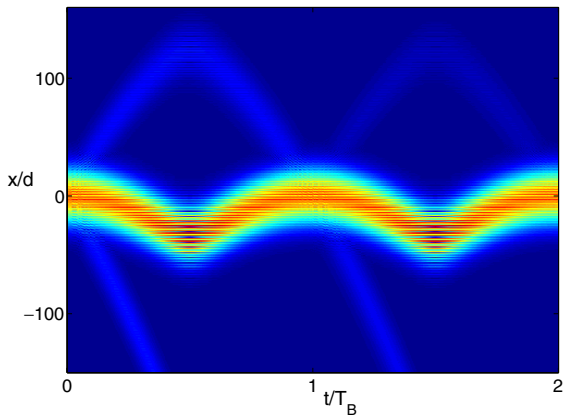

Figure 8. Bloch oscillations in co-ordinate space for $F = 0.005$ and $\hbar = 3.3806$.

can be quite easily solved numerically by means of a split-operator technique [47]. Scaled variables are used where the values of M and V_0 are unity, $d = 2\pi$ and the value of the scaled $\hbar$ is related to the original values by $2\pi\hbar/d\sqrt{MV_0}$ [5].

The value of the scaled Planck constant was chosen as $\hbar = 3.3806$ which corresponds to the experimental situation in [21]. In order to reduce the decay probability, however, the field was chosen as $F = 0.005$, which is considerably less than the value of $F = 0.0661$ in the experiment (for a theoretical treatment of this strongly decaying system see [48]). As an initial wavepacket, we use a normalized minimum uncertainty Gaussian wavepacket with width $\Delta x_0 = 80\pi$ centred at $x_0 = 0$ and zero initial momentum, i.e. about 40 potential wells are coherently populated initially. In the Kasevich experiment [21], this has been achieved by means of a (diluted) Bose–Einstein condensate, but it may also be obtained by initial driving as suggested in [48]. As discussed for the tight-binding model in section 2, the momentum localization is important for the dynamics. Here we will choose a wavepacket sharply localized in momentum with $\Delta k = 1/(2\Delta x) = 1/(160\pi)$.

Figure 8 shows the dynamics in co-ordinate space as a function of time (shown is the density $|\psi(x,t)|^2$ over two Bloch periods where the bright regions are strongly populated). At $t = 0$, the wavepacket splits immediately into three parts: the main part moves in the negative x-direction, oscillating with the Bloch frequency, a second weaker fraction oscillates in the opposite direction with a larger amplitude and the third fraction decays towards infinity. The splitting is repeated after multiples of the Bloch time T_B. This behaviour can be described by two models. First, since the field F is weak, the Wannier states $|\psi_{\alpha,m}\rangle$ can still be considered as a basis for the system. Neglecting the interband coupling, this leads to the single band or, more restrictively, to the tight-binding system described in section 2. However, the field F destroys the (discrete) translational invariance of the field-free Hamiltonian and consequently the Bloch bands. The full Wannier–Stark system shows, instead of bands, discrete resonance energy levels with an imaginary part describing the decay of these states (see e.g. [5]). We will analyse the Bloch oscillations in both approaches, because each has advantages in describing certain phenomena.

In the band model, the oscillation of the wavepacket reflects the periodicity of the band structure. Figure 9 shows the four lowest bands of the field-free system. A wavepacket localized around $\kappa = 0$ moves in quasi-momentum space according to the Bloch equation (14). The width of the ground band is computed as $\Delta \approx 0.994$, which yields according to

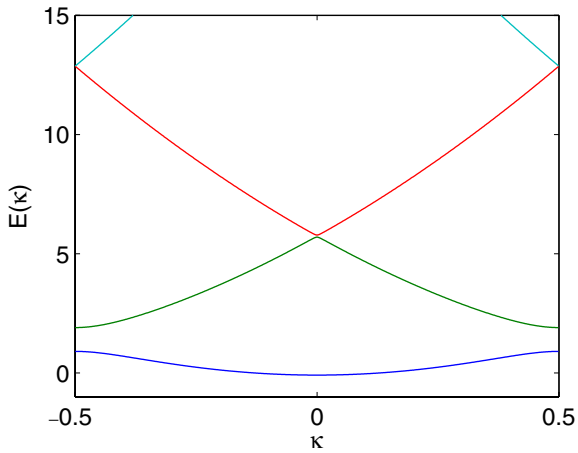

Figure 9. Dispersion relation for a potential $V(x) = \cos x$ and $\hbar = 3.3806$. Shown are the four lowest bands in the first Brillouin zone. Bandwidths of the ground and first excited bands are 0.994 and 3.794, and the band gaps are 0.998 and 0.086, respectively.

equation (51) an oscillation over $L/d = \Delta/(Fd) \approx 32$ periods in agreement with the numerical propagation in figure 8. The numerically observed splitting of the wavepacket (see figure 8) is due to the fact that the initial Gaussian wavepacket has perceptible contributions from the first and second excited band. If the initial Gaussian is first projected onto the ground band $|\psi_{\alpha=0,n}\rangle$, the subsequent time evolution is much clearer as shown on the left-hand side of figure 10. The projection on the first and second excited band (right-hand side of figure 10) shows a splitting into two wavepackets. The reason for this is the tiny band gap of 0.086 at $\kappa = 0$ (see figure 9) and so the wavepacket immediately splits into two fractions. The part belonging to the first excited band has a group velocity

$$v_g = \frac{1}{\hbar}\frac{\partial E(\kappa)}{\partial \kappa} \tag{77}$$

which is positive for $\kappa < 0$ and oscillates therefore in the positive direction, whereas the second excited band has a negative group velocity and decays to $-\infty$, i.e. it tunnels through the upper bands. The spatial amplitude of the Bloch oscillation in the first excited band is increased by a factor of 3.8 because of the larger width $\Delta = 3.794$ (see figure 9 and equation (51)).

Alternatively, the dynamics can be described in terms of the resonance states [5] of the Wannier–Stark Hamiltonian (1). In this so-called rigged Hilbert space, the Hamiltonian is not hermitian and so the eigenenergies have an imaginary part that can be interpreted as the decay probability (for a calculation method of these Wannier–Stark resonances, see e.g. [6]). Due to the symmetry of the system, the eigenenergies and eigenstates, the so-called Wannier–Stark states, fulfil the relations

$$\mathcal{E}_{\alpha,n} = \mathcal{E}_{\alpha,0} + ndF, \qquad \Psi_{\alpha,n}(x) = \Psi_{\alpha,0}(x - nd), \qquad \alpha \in \mathbb{N}_0, \quad n \in \mathbb{Z}. \tag{78}$$

The complex energies $\mathcal{E}_{\alpha,0}$ can be decomposed as $\mathcal{E}_{\alpha,0} = E_{\alpha,0} - \mathrm{i}\Gamma_\alpha/2$. The decay rate of the resonance is given by $\Gamma_\alpha/\hbar$. Figure 11 shows for $F = 0.005$ the most stable state $\alpha = 0$ for

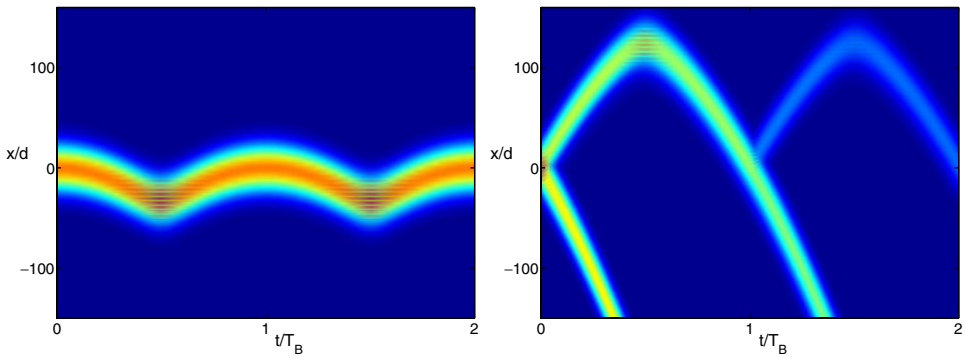

Figure 10. Propagation of a Gaussian wavepacket projected on the ground band (a) and the first plus second excited band (b) initially. The absolute value of the wavefunction has been plotted.

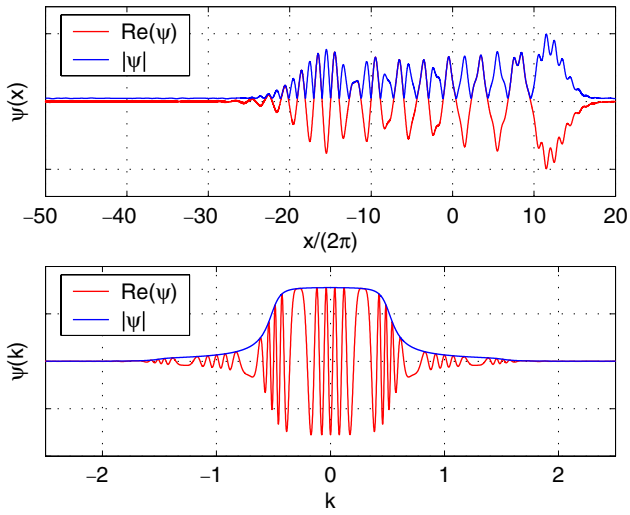

Figure 11. Wannier–Stark state $\Psi_{0,0}$ in co-ordinate (top) and momentum space (bottom) for $F = 0.005$, $\hbar = 3.3806$. Shown are the absolute values and the real parts.

site $n = 0$ both in the co-ordinate (top) and momentum representation (bottom). We first note the close similarity to the results of the tight-binding model in figure 2 which were calculated for the parameter $\gamma = \Delta/2dF = 15.8$. The wavefunction shows fast oscillations with the period $d = 2\pi$ of the potential which increases in amplitude from $x \approx 0$ to $x \approx -L = -\Delta/F$. Note that (as expected), mainly the potential minima are populated. Note further the change in sign between the minima on the left turning point of the Bloch oscillation.

The momentum representation $\psi_{00}(k)$, i.e. the Fourier transform of $\psi_{00}(x)$, shown in figure 12 (bottom) is mainly localized in the Brillouin zone $|k| \leqslant b/2 = 1/2$. One can see the close similarity to the Wannier functions of the field-free case in figure 7. Since the other Wannier–Stark states $\Psi_{0,m}$ of the ground ladder are simply shifted by m periods $\Psi_{0,m}(x) = \Psi_{0,0}(x - md)$, the momentum wavefunctions are multiplied by a phase factor, $\Psi_{0,m}(k) = \mathrm{e}^{-\mathrm{i}mkd}\Psi_{0,0}(k)$, i.e. $|\Psi_{0,m}(k)| = |\Psi_{0,0}(k)|$.

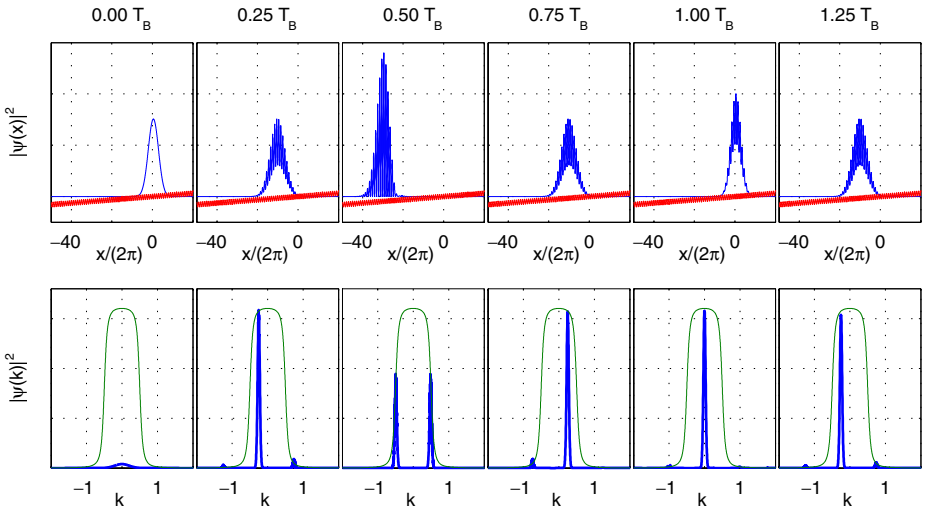

Figure 12. Time evolution of the absolute value of a Gaussian wavepacket in co-ordinate (top) and momentum space (bottom). The field strength is $F = 0.005$ and $\hbar = 3.3806$. In the momentum representation, the absolute value of the Wannier–Stark function $|\Psi_{0,0}(k)|$ is shown as a green line. See animation.

For the same parameters, the numerically computed time evolution of an initial Gaussian wavepacket (width $\Delta x_0 = 100$) centred at $x_0 = 0$ and zero initial momentum is shown in figure 12 (see also the animation). The motion in co-ordinate space (top) shows a Bloch oscillation with period T_B extending over $L/d \approx 32$ periods of the potential. We observe, however, that this is *not* a strictly periodic motion, because after a time T_B the initial Gaussian is not entirely reconstructed. As already discussed above, a fraction of the initial wavefunction is transferred to the upper Wannier–Stark ladders and escapes.

The time evolution of an arbitrary initial state can be conveniently written as

$$|\psi(t)\rangle = \sum_{\alpha,m} |\Psi_{\alpha,m}\rangle\langle\Psi_{\alpha,m}|\psi(0)\rangle\, \mathrm{e}^{-\mathrm{i}\mathcal{E}_{\alpha,m}t/\hbar} \tag{79}$$

with $\mathcal{E}_{\alpha,m} = \mathcal{E}_{\alpha,0} + 2\pi Fm$. If the initial state only occupies a single ladder α (which will be quite generally the ground state if we wait long enough until the contributions from the more unstable states have decayed) the dynamics simplifies, in particular in the momentum representation, where (79) can be cast into the form [48]

$$\begin{aligned}\psi(k,t) &= \mathrm{e}^{-\mathrm{i}\mathcal{E}_{\alpha,0}t/\hbar}\Psi_{\alpha,0}(k)\sum_m c_{\alpha,m}\exp(-2\pi\mathrm{i}m(k+Ft/\hbar)) \\ &= \mathrm{e}^{-\mathrm{i}\mathcal{E}_{\alpha,0}t/\hbar}\Psi_{\alpha,0}(k,0)C_\alpha(k+Ft/\hbar) = \Psi_{\alpha,0}(k,t)C_\alpha(k+Ft/\hbar)\end{aligned} \tag{80}$$

(cf relation (74)). Up to the exponential factor, the dynamics appears in the amplitude modulation function $C_\alpha(k)$, the discrete Fourier transform of the initial occupation coefficients. It is a periodic function with period $b = 2\pi/d = 1$. Therefore, up to an overall damping due to the imaginary part of the resonance energy $\mathcal{E}_{\alpha,0}$, the probability distribution $|\psi(k,t)|^2$ reproduces itself after

multiples of the Bloch time $T_B = 2\pi\hbar/dF$. The damping factor

$$|\exp(-\mathrm{i}\mathcal{E}_{\alpha,0}T_B/\hbar)| = \exp(-\Gamma_\alpha/(2F)) \tag{81}$$

plays a role if the exponent is of the order unity, which is already the case for $\alpha = 1$. Therefore the Gaussian wavepacket is not exactly reproduced after the first Bloch period and the contributions of the higher bands are already lost.

As an example, let us discuss an initial Gaussian occupation of the Wannier–Stark ladder α, i.e.

$$c_{\alpha,m} = g\exp(-\beta m^2) \tag{82}$$

(see also (22)). Using the well-known θ-transformation [49], $C_\alpha(k)$ can be explicitly evaluated to give

$$C_\alpha(k) = g\sqrt{\frac{\pi}{\beta}}\sum_m \exp\left(-\frac{\pi^2}{\beta}(k-mb)^2\right) \tag{83}$$

and the full-time evolution in the single-resonance ladder approximation is given by

$$\psi(k,t) = g\sqrt{\frac{\pi}{\beta}}\,\mathrm{e}^{-\mathrm{i}\mathcal{E}_{\alpha,0}t/\hbar}\Psi_{\alpha,0}(k)\sum_m \exp\left(-\frac{\pi^2}{\beta}(k+Ft/\hbar-mb)^2\right). \tag{84}$$

Therefore, we expect a comb of equidistant equal Gaussians moving with constant width and speed centred at $k_m(t) = mb - Ft/\hbar$ which are multiplied by the overall k-distribution $|\Psi_{\alpha,0}(k)|^2$ of the Wannier–Stark state localized mainly in the interval $|k| \leqslant b/2$. The momentum peaks outside this region rapidly disappear. At $t = 0$, the most prominent peak appears at $k = 0$. After half of a Bloch period, we have two symmetric peaks at $k = \pm b/2$ whose height is reduced by the factor $|\Psi(k = \pm b)/\Psi(k = 0)|$. This is exactly what is observed in the numerical solutions shown in figure 12 and also in the animation. Let us finally note that the average momentum is zero, both for $t = 0$ and $t = T_B/2$, due to the symmetry of the distribution at these times. There is an essential difference, however. In the first case, the momentum distribution peaks at the centre of the Brillouin zone, whereas in the latter case we have two counterpropagating waves with momenta at the boundary of the Brillouin zone.

The mean value of the momentum

$$\langle k\rangle_t = \int_{-\infty}^{+\infty} \mathrm{d}k\, k|\psi(k,t)|^2 \tag{85}$$

calculated numerically from the wavepacket propagation is shown in figure 13 for the data of figure 12. The prominent feature of this periodic oscillation is its asymmetry, as already observed and discussed in experimental measurements of Bloch oscillations of ultracold atoms [12]–[14]. This asymmetry can be understood by means of the momentum distributions shown in figure 12 and reflects the shape of the envelope function $|\Psi_{\alpha,0}(k)|$: if this distribution is rectangular, $\langle k\rangle_t$ would be a sawtooth function and the smoothed steps in $|\Psi_{\alpha,0}(k)|$ lead to a corresponding smoothing of the sawtooth. More intuitive, however, is an alternative approach

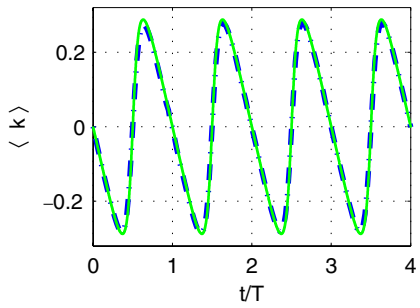

Figure 13. The time evolution of the mean value of the momentum $\langle k \rangle$ for the wavepacket propagation shown in figure 12 (solid curve) is well reproduced by the single-band group velocity (86) (dashed curve).

(see also [12]–[14]): in the single-band model (see section 2.3), the group velocity $v_g(\kappa)$ in (77) can be calculated from the dispersion relation $E(\kappa)$ of the ground band shown in figure 9. The mean momentum is then given by

$$\langle k \rangle_t \approx M v_g(\kappa(t))/\hbar, \qquad \kappa(t) = \kappa(0) - Ft/\hbar. \tag{86}$$

This 'classical' momentum oscillation, also shown in figure 13, almost perfectly reproduces the exact quantum result (see also the similar observation in [50]). Let us finally point out that the underlying physics is exactly what has been discussed in Bloch's original paper [2].

The time evolution in co-ordinate space is more difficult to describe. By a direct expansion in Wannier–Stark states

$$\psi(x,t) = \sum_m c_{\alpha,m} \Psi_{\alpha,m}(x,t) = \mathrm{e}^{-\mathrm{i}\mathcal{E}_{\alpha,0}t/\hbar} \sum_m c_{\alpha,m}\, \mathrm{e}^{-\mathrm{i}mdFt/\hbar} \Psi_{\alpha,0}(x - md), \tag{87}$$

we see that the contributions from the Wannier–Stark functions of each well are summed with a time-dependent phase factor. At time $t = 0$, we have simply a sum of copies of the Wannier–Stark functions shown in figure 11 displaced by m potential wells. Assuming positive weight factors $c_{\alpha,m}$, this summation is constructive around $x = 0$ and destructive around $x = -L$ because the Wannier–Stark function changes sign from one well to the next and the contributions from term m and $m + 1$ cancel if the weight coefficients $c_{\alpha,m}$ change slowly. At time $t = T_B/2$, the phase factors are $(-1)^m$ and thus the inverse behaviour is observed: the interference is destructive around $x = 0$ and constructive around $x = -L$.

A different approach may provide some more insight. Starting from (80), we get the co-ordinate space representation by evaluating the integral

$$\psi(x,t) = \frac{1}{\sqrt{2\pi}} \int_{-\infty}^{+\infty} \mathrm{d}k\, \mathrm{e}^{\mathrm{i}kx} \Psi_{\alpha,0}(k,t)\, C_\alpha(k + Ft/\hbar). \tag{88}$$

Using the convolution theorem, this reduces to

$$\psi(x,t) = \int_{-\infty}^{+\infty} \mathrm{d}x' \Psi_{\alpha,0}(x',t) \widetilde{C}_\alpha(x - x', t), \tag{89}$$

where $\widetilde{C}_\alpha(x,t)$ is the Fourier transform of $C_\alpha(k+Ft/\hbar)$. This Fourier transform can be evaluated to give

$$\psi(x,t) = \frac{g}{\sqrt{2\pi}} \mathrm{e}^{-\mathrm{i}\mathcal{E}_{\alpha,0}t/\hbar} \sum_m \int_{-\infty}^{+\infty} \mathrm{d}x' \Psi_{\alpha,0}(x',0) \times \exp\left(-\frac{16\beta}{d^2}(x-x')^2 + \mathrm{i}(mb - Ft/\hbar)(x-x')\right). \tag{90}$$

We see that the time-developed state $\psi(x,t)$ consists of a superposition of windowed Fourier or Gabor transformations

$$\Phi_\alpha(x,k) = \frac{1}{\sqrt{2\pi}} \int_{-\infty}^{+\infty} \mathrm{d}x' \Psi_{\alpha,0}(x',0) \exp\left(-\frac{16\beta}{d^2}(x-x')^2 + \mathrm{i}k(x-x')\right) \tag{91}$$

which describe the local wavenumber spectrum of $\Psi_{\alpha,0}(x',0)$ at $x'=x$:

$$\psi(x,t) = g\,\mathrm{e}^{-\mathrm{i}\mathcal{E}_{\alpha,0}t/\hbar} \sum_m \Phi_\alpha(x,k_m(t)), \qquad k_m(t) = mb - Ft/\hbar. \tag{92}$$

Around $x=0$, the $\Psi_{\alpha,0}$ is non-oscillatory, i.e. only small values of k contribute, contrary to the region $x \approx L$, where the dominant wavenumbers are $\pm b/2$, i.e. we have two counterpropagating waves of the same amplitude, which yield a standing wave with period $2\pi/(b/2) = 2d$. The total wavefunction at time t is a superposition of these contributions from all $k_m(t)$ and we obtain a time-dependent scanning of the underlying Wannier–Stark function $\Psi_{\alpha,0}(x,0)$. Because of $k_m(t+T_B) = k_{m-1}(t)$ this motion is periodic.

4. Concluding remarks

In this paper, we have presented numerical studies of Bloch oscillations in one-dimensional systems where the force F is weak and does not depend explicitly on time. Even in this simple set-up, the dynamics is quite involved as discussed above. A feature of particular interest is the dispersionless periodic oscillation of a wavepacket with an amplitude $L = \Delta/F$ and a period $T_B = 2\pi\hbar/dF$, at least in the limit of small fields F. For stronger fields, the coupling between the bands is enhanced and an increasing fraction of the wavepacket moves in higher bands and finally escapes. In this regime, a description in terms of Wannier–Stark resonance states [5] is more adequate. An application to a situation with an intermediate field F can be found in the experiment [21] where a pulsed coherent emission of a Bloch-oscillating Bose–Einstein condensate was observed (see also the theoretical analysis [48]).

If we allow for an additional time-periodic driving many other phenomena occur. An example is the classically chaotic motion with corresponding signatures in the quantum case, as for instance statistical properties of the decay rates or resonance widths which can be described by random matrix theory (see the review [5] and references therein). Other interesting questions are related to transport phenomena. Let us, for instance, have a brief look at an alternating field F where we change sign after half of the first Bloch period, i.e. at the left-hand-side turning point (cf with figure 12). This will invert the direction of the Bloch oscillation and the wavepacket will continue its motion in the *same* direction as in the first half-period. If we continue to flip the

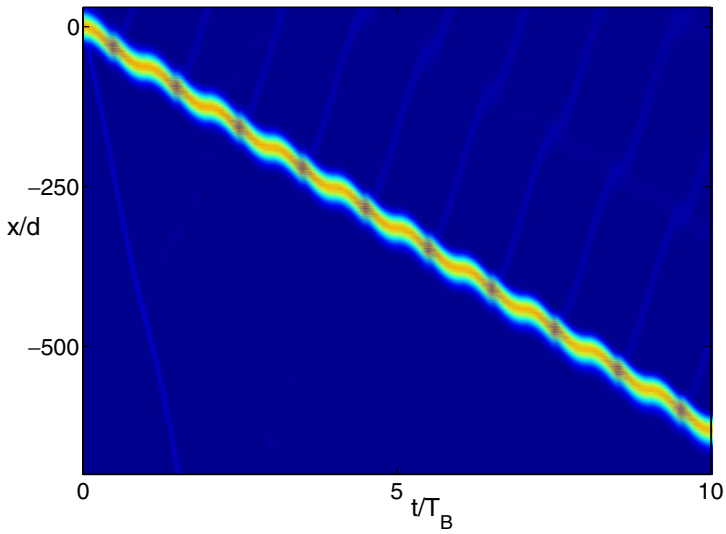

Figure 14. Propagation of a Gaussian wavepacket with a T_B-periodically flipped field $|F| = 0.005$.

sign of F after each half-period, the resulting motion will be in the same direction all the time. Figure 14 shows a numerical propagation of a Gaussian wavepacket under the action of such a T_B periodic force.

Each time the boundary of the Brillouin zone is met, a small fraction of the wavepacket escapes. The main part of the wavepacket moves, but is almost dispersionless. Estimating the transport velocity v, we obtain

$$v = \frac{2L}{T_B} = \frac{\Delta d}{\pi\hbar} \tag{93}$$

which is *independent* of the magnitude $|F|$ of the force. The direction of the transport depends only on the initial sign of F. This is clearly a non-intuitive behaviour which will be analysed in future studies of transport processes in driven Wannier–Stark systems.

Even more interesting is the dynamics of Wannier–Stark systems in two (and more) space dimensions. A few recent studies have shown a sensitive dependence of the motion (dispersion and decay characteristics) on the direction of the field with respect to the periodic lattice. In addition, an almost dispersionless motion of wavepackets has been found. This will be discussed in a subsequent paper [51].

Acknowledgments

Support from the Deutsche Forschungsgemeinschaft via the Graduiertenkolleg 'Nichtlineare Optik und Ultrakurzzeitphysik' as well as from the Volkswagen Foundation is gratefully acknowledged.

References

[1] Zener C 1934 *Proc. R. Soc.* A **145** 523
[2] Bloch F 1928 *Z. Phys.* **52** 555

[3] Holthaus M 2000 *J. Opt. B: Quantum Semiclass. Opt.* **2** 589
[4] Grecchi V and Sacchetti S 2001 *Phys. Rev.* B **63** 212303
[5] Glück M, Kolovsky A R and Korsch H J 2002 *Phys. Rep.* **366** 103
[6] Glück M, Kolovsky A R and Korsch H J 1999 *J. Phys. A: Math. Gen.* **32** L49
[7] Waschke C, Roskos H G, Schwedler R, Leo K, Kurz H and Köhler K 1993 *Phys. Rev. Lett.* **70** 3319
[8] Dekorsy T, Leisching P, Köhler K and Kurz H 1994 *Phys. Rev.* B **50** 8106
[9] Cho G C, Dekorsy T, Bakker H J, Kurz H, Kohl A and Opitz B 1996 *Phys. Rev.* B **54** 4420
[10] Lyssenko V G, Valusis G, Löser F, Hasche T and Leo K 1997 *Phys. Rev. Lett.* **79** 301
[11] Leo K 1998 *Semicond. Sci. Technol.* **13** 249
[12] Ben Dahan M, Peik E, Reichel J, Castin Y and Salomon C 1996 *Phys. Rev. Lett.* **76** 4508
[13] Peik E, Dahan M B, Bouchoule I, Castin Y and Salomon C 1997 *Phys. Rev.* A **55** 2989
[14] Peik E, Dahan M B, Bouchoule I, Castin Y and Salomon C 1997 *Appl. Phys.* B **65** 685
[15] Niu Q, Zhao X-G, Georgakis G A and Raizen M G 1996 *Phys. Rev. Lett.* **76** 4504
[16] Wilkinson S R, Bharucha C F, Madison K W, Niu Q and Raizen M G 1996 *Phys. Rev. Lett.* **76** 4512
[17] Bharucha C F, Madison K W, Morrow P R, Wikinson S R, Sundaram B and Raizen M G 1997 *Phys. Rev.* A **55** R857
[18] Madison K W, Bharucha C F, Morrow P R, Wilkinson S R, Niu Q, Sundaram B and Raizen M G 1997 *Appl. Phys.* B **65** 693
[19] Madison K W, Fischer M C and Raizen M G 1999 *Phys. Rev.* A **60** R1767
[20] Raizen M G, Salomon C and Niu Q 1997 *Phys. Today* **50** 30
[21] Anderson B P and Kasevich M A 1998 *Science* **282** 1686
[22] Morsch O, Müller J H, Cristiani M, Ciampini D and Arimondo E 2001 *Phys. Rev. Lett.* **87** 140402
[23] Cristiani M, Morsch O, Müller J H, Ciampini D and Arimondo E 2002 *Phys. Rev.* A **65** 063612
[24] Peschel U, Pertsch T and Lederer F 1998 *Opt. Lett.* **23** 1701
[25] Pertsch T, Dannberg P, Elflein W, Bräuer A and Lederer F 1999 *Phys. Rev. Lett.* **83** 4752
[26] Morandotti R, Peschel U, Aitchinson J S, Eisenberg H S and Silberberg Y 1999 *Phys. Rev. Lett.* **83** 4756
[27] Pertsch T, Zentgraf T, Peschel U, Bräuer A and Lederer F 2002 *Phys. Rev. Lett.* **88** 093901
[28] Pertsch T, Zentgraf T, Peschel U, Bräuer A and Lederer F 2002 *Ann. Phys., Lpz* **80** 3247
[29] Wilkinson P B 2002 *Phys. Rev.* E **65** 056616
[30] Kyriakidis J and Loss D 1998 *Phys. Rev.* B **58** 5568
[31] Dekorsy T, Bartels A, Kurz H, Köhler K, Hey R and Ploog K 2000 *Phys. Rev. Lett.* **85** 1080
[32] Rotvig J, Jauho A-P and Smith H 1995 *Phys. Rev. Lett.* **74** 1831
[33] Holthaus M and Hone D W 1996 *Phil. Mag.* B **74** 105
[34] Grifoni M and Hänggi P 1998 *Phys. Rep.* **304** 229
[35] Abramowitz M and Stegun I A 1972 *Handbook of Mathematical Functions* (New York: Dover)
[36] Fukuyama H, Bari R A and Fogedby H C 1973 *Phys. Rev.* B **8** 5579
[37] Dunlap D H and Kenkre V M 1986 *Phys. Rev.* B **34** 3625
[38] Korsch H J and Mossmann S 2003 *Phys. Lett.* A **317** 54
[39] Goychuk I, Grifoni M and Hänggi P 1998 *Phys. Rev. Lett.* **81** 649
[40] Goychuk I and Hänggi P 2000 *Stochastic Processes in Physics (Lecture Notes in Physics* vol. 557*)* eds J Freund and T P Pöschel (Berlin: Springer) p 7
[41] Carruthers P and Nieto M M 1968 *Rev. Mod. Phys.* **40** 411
[42] Kowalski K, Rembieliński J and Papaloucas L C 1996 *J. Phys. A: Math. Gen.* **29** 4149
[43] Grecchi V and Sacchetti A 1998 *Comput. Math. Phys.* **197** 553
[44] Houston W V 1940 *Phys. Rev.* **57** 184
[45] Kohn W 1959 *Phys. Rev.* **115** 809
[46] Bouchard A M and Luban M 1995 *Phys. Rev.* B **52** 5105
[47] Feit M D, Fleck Jr J A and Steiger A 1982 *J. Comput. Phys.* **47** 412

[48] Glück M, Keck F and Korsch H J 2002 *Phys. Rev.* A **66** 043418
[49] Remmert R 1991 *Theory of Complex Functions* (Berlin: Springer)
[50] Kolovsky A R, Ponomarev A V and Korsch H J 2002 *Phys. Rev.* A **66** 053405
[51] Witthaut D, Keck F, Korsch H J and Mossmann S 2004 *New J. Phys.* (in preparation)